



**Cite this article:** Goldstein RE, van de Meent J-W. 2015 A physical perspective on cytoplasmic streaming. *Interface Focus* 5: 20150030.  
<http://dx.doi.org/10.1098/rsfs.2015.0030>

One contribution of 10 to a theme issue 'Bioinspiration of new technologies'.

**Subject Areas:**  
biophysics, biomechanics

**Keywords:**  
cytoplasmic streaming, cell size, transport

**Author for correspondence:**  
Raymond E. Goldstein  
e-mail: [r.e.goldstein@damtp.cam.ac.uk](mailto:r.e.goldstein@damtp.cam.ac.uk)

# A physical perspective on cytoplasmic streaming

Raymond E. Goldstein<sup>1</sup> and Jan-Willem van de Meent<sup>2</sup>

<sup>1</sup>Department of Applied Mathematics and Theoretical Physics, Centre for Mathematical Sciences, University of Cambridge, Wilberforce Road, Cambridge CB3 0WA, UK

<sup>2</sup>Department of Engineering Science, University of Oxford, Parks Road, Oxford OX1 3PJ, UK

Organisms show a remarkable range of sizes, yet the dimensions of a single cell rarely exceed 100  $\mu\text{m}$ . While the physical and biological origins of this constraint remain poorly understood, exceptions to this rule give valuable insights. A well-known counterexample is the aquatic plant *Chara*, whose cells can exceed 10 cm in length and 1 mm in diameter. Two spiralling bands of molecular motors at the cell periphery drive the cellular fluid up and down at speeds up to 100  $\mu\text{m s}^{-1}$ , motion that has been hypothesized to mitigate the slowness of metabolite transport on these scales and to aid in homeostasis. This is the most organized instance of a broad class of continuous motions known as 'cytoplasmic streaming', found in a wide range of eukaryotic organisms—algae, plants, amoebae, nematodes and flies—often in unusually large cells. In this overview of the physics of this phenomenon, we examine the interplay between streaming, transport and cell size and discuss the possible role of self-organization phenomena in establishing the observed patterns of streaming.

## 1. Transport and cell size in biology

Relative to the remarkable variation of sizes exhibited by living organisms, the dimensions of a typical cell are surprisingly similar across species. In nearly all plant-like multicellulars the constituent cells measure 10–100  $\mu\text{m}$ , with animal cells falling into a similar if slightly smaller range and single-cellular prokaryotes extending down to 1  $\mu\text{m}$ . Thus, outside of a few notable exceptions the overwhelming majority of organisms have cell sizes in the range 1–100  $\mu\text{m}$ . A very basic question about the fundamentals of cellular biology is: what underlying mechanism has determined the evolution of this relatively well-conserved length scale?

The fact that very few cells are larger than 100  $\mu\text{m}$  suggests that this size reflects physical constraints, such as the diffusive range over which two metabolites can reliably interact. The outliers showing larger cell sizes provide key counterexamples, prompting the question of how these species have compensated for problems associated with an increasing cell size, and what utility this design provides in an evolutionary context. In some cases, large sizes are found in cells with a highly specialized role. The nerve fibres in our body can reach lengths of a metre, and the *giant squid axon* can have a diameter up to 1 mm, improving the propagation speed of the action potentials which ultimately facilitates a faster escape response. In other cases, single-cellular organisms have evolved to a large size and complexity. Examples of this are the protozoan *Paramecium*, which can reach 350  $\mu\text{m}$ , and the trumpet-shaped *Stentor* (2 mm). Arguably even more developed is the alga *Acetabularia*, a single-cellular organism that grows into a plant-like stalk that can be as long as 10 cm. Finally, there are the characean algae, a family of plant-like weeds whose segmented stems are built up out of cylindrical *internodal cells* of 200–1000  $\mu\text{m}$  diameter and lengths that can exceed 10 cm.

Cells in these examples have the common feature of forms of active internal transport, driven by the movement of *molecular* motors along intracellular

filaments that make up the *cytoskeleton*. In small cells, this motion enables movement of organelles and vesicles. In larger cells, it leads to a continuous circulation of the cellular fluid, known as *cytoplasmic streaming* or *cyclosis*. Streaming is found in many types of larger eukaryotic cells, particularly in plants [1]. Patterns of circulation take on a variety of geometric forms and can be very steady.

Cytoplasmic streaming has long been conjectured to aid in overcoming the slowness of diffusion on long length scales, but its precise role in enhancing metabolic rates is yet to be elucidated. This article provides an overview of the current state of knowledge surrounding this issue. Over the last two decades, our understanding of the molecular make-up and spatial organization of the cellular environment has increased dramatically. We begin with an overview of how spatial aspects of intracellular transport factor in to our understanding of metabolic regulation. This is followed by an explanation of the range of topologies of circulation found across species. The arguably best studied instance of this phenomenon is the *rotational* streaming found in the long cylindrical cells of the characean algae, whose metabolic context is covered in detail. We conclude with a discussion of those studies that have investigated the role of circulation in intracellular transport and provide an overview of key questions in furthering our understanding of how streaming enables enhanced diffusive transport.

### 1.1. Homeostasis and targeting of macromolecules

Cellular life requires precise control of metabolic pathways and biosynthesis. Two central challenges in internal regulation are the maintenance of *homeostasis* and the control of *trafficking*. In metabolic pathways, turnover rates can vary by several orders of magnitude. The dynamic equilibrium of a biological system's properties in the face of fluctuating levels of throughput is generally termed homeostasis [2]. The concept of homeostatic control necessarily encompasses a range of regulatory mechanisms, whose function is often specific to the type of organism considered. In mammals, key homeostatic requirements are the regulation of body temperature and the stabilization of oxygen pathways and cellular ATP levels under varying levels of muscle activity [3]. In plants, homeostatic control is associated with turgor pressure and cytosolic concentrations of inorganic ions such as calcium and phosphate [4], as well as cellular building blocks such as amino acids.

In addition to homeostatic regulation, which predominantly involves concentrations of small molecules, intracellular transport of proteins, lipids and polysaccharides requires a high degree of targeting [5–8]. Eukaryotic cells possess an array of organelles, each containing a distinct set of proteins that allow it to perform its biochemical activities. The translation of nearly all cellular proteins takes place in the cytoplasm, after which they must be targeted to one of more than 30 compartments in the cell [5]. The mechanisms for targeting form a central area of inquiry in cell biology and have been studied intensively in recent years. We now know that each protein contains a targeting domain in its amino acid sequence, which interacts with receptors on the organelle to which it is to be transported. Additionally, many macromolecules are transported between organelles inside lipid vesicles, with a differentiated coating, as well as a SNARE marker protein to identify its contents [8].

Two organelles that play a central role in protein synthesis are the endoplasmic reticulum (ER) and the Golgi apparatus. The ER is a network of continuous tubules that courses through the cytoplasm. Comprising as many as 16 functionally distinct subdomains, it fulfils a multitude of roles in cellular metabolism and in some species extends between cells through the channels known as plasmodesmata [9]. The ER is the entry point for newly synthesized proteins into the trafficking network of membrane-bound organelles known as the endomembrane system. Inside the ER, polypeptides created by ribosomal translation are folded into soluble proteins by means of the chaperone BiP [8]. Typically, protein products from the ER are subsequently extruded in vesicles and transported to the Golgi apparatus for further sorting and processing. Storage proteins, for example those used as nutrients in seed formation, can also bypass the Golgi apparatus to be stored in protein storage vacuoles (PSVs) by way of intermediate compartments [8].

The plant Golgi apparatus plays a central role in protein processing and sorting, but also synthesizes large quantities of cell wall polysaccharides and glycolipids for inclusion in the plasma membrane [7,8,10]. Plant cells can have tens to hundreds of Golgi stacks, which are often closely associated with the ER network and are known to localize to specific subcellular regions in cell types exhibiting localized cell wall growth [10].

### 1.2. Diffusion in a crowded cytoplasm

In formulating an understanding of trafficking and homeostatic control, it is becoming increasingly apparent that many transport processes in cells require explanation [3,11,12]. In the past, a simplified picture of a cell as a watery bag of enzymes has often been invoked for lack of a more detailed model. This metaphor has given way to the notion of a highly crowded and highly structured cytoplasm, requiring a spatial (and chemical) understanding of metabolic pathways. As demonstrated in a comprehensive review by Luby-Phelps [13], a number of assumptions valid for chemical reactions in an aqueous environment break down in the cytoplasm.

#### 1.2.1. Reaction volumes are small

While biochemical analysis typically neglects finite-volume effects, key molecules *in vivo* are often only present in limited numbers. Physiologically relevant concentrations tend to lie in the nanomolar to millimolar range. A single molecule inside a bacterium has a nominal concentration of 10 nM, while eukaryotic cells may possess perhaps only 1000 copies of a molecular species [14]. Thus, the number concentration of subcellular compartments may in many cases be more informative than the nominal molar concentration.

#### 1.2.2. The cytoplasm is a crowded environment

In a cellular environment, macromolecules typically occupy 20–30% of the total volume [15], leading to a range of phenomena known together as *macromolecular crowding* [13,15–17]. Figure 1 shows an iconic visualization of the cytoplasmic environment in baker's yeast [18]. Cellular components such as proteins and ribosomes are all shown at correct scale and density, along with cytoskeletal elements. While 70–80% of the volume is water, it is clear that diffusive movement will be constrained in a manner that will depend strongly on particle size.

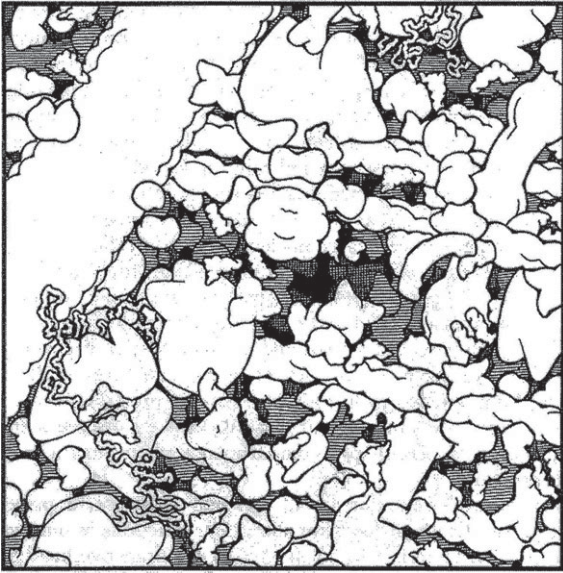


**Figure 1.** Molecular crowding in eukaryotic cytoplasm. Shown is an illustration of the contents of the yeast *Saccharomyces cerevisiae*. Proteins, ribosomes with mRNA, microtubules, actin filaments and intermediate filaments are all drawn to scale and at physiological concentrations. (Adapted with permission from [18].)

This intuitive notion is borne out by experimental evidence. Measurements of mobility of water in living tissue by NMR and quasi-elastic neutron scattering (QENS) show a reduction of the order of 50% of both rotational and translational diffusion [13,19–21]. Self-diffusion of larger macromolecules shows a strong reduction in mobility that depends on the hydrodynamic radius [13,22], declining from 40% to 5% of the aqueous diffusion rate for particle sizes increasing from 2 to 45 nm [13,23–26]. More recently, several studies have presented evidence of *anomalous diffusion* in the cytoplasm: particle trajectories show a mean-squared displacement that is subdiffusive, i.e.  $\langle r^2(t) \rangle \sim t^\alpha$  with  $\alpha < 1$  [27–30]. For larger vesicles, the diffusion rates are of order  $10^{-11} \text{ cm}^2 \text{ s}^{-1}$ , implying that vesicular movement will be insignificant in the absence of active transport mechanisms [13].

### 1.2.3. The cytoplasm is highly structured and compartmentalized

It is increasingly recognized that the cytoplasm is not a homogeneous environment. Macromolecular crowding effects may well result in separation of the cytoplasmic volume into distinct microphases, as evidenced from phenomena such as caged diffusion of microinjected beads and the size-dependent partitioning of inert tracers [13].

### 1.3. Motor-driven transport along the cytoskeleton

In the spatial organization of a cell, the *cytoskeleton* plays a central role. This meshwork of *actin*, intermediate filaments and *microtubules* acts as a backbone for directed transport. Myosin molecular motors can bind to cytoplasmic structures and transport them along actin filaments by a ‘walking’ motion that consumes ATP. Microtubules have kinesin and dynein motors that perform similar tasks. The filaments that make up the cytoskeleton are polar, in the sense that molecular motors move in a well-defined direction along their tracks. Whereas the various myosins walk along actin in directions that depend on their type, kinesins walk towards the plus end of microtubules, which typically results in transport

from the cell centre towards the periphery. Dyneins travel in the opposite direction. The topology of the cytoskeleton thus defines the direction of motor-assisted transport.

The forms of active transport observed depend greatly on the organism and cell type. In animal cells, which tend to be small compared with their plant counterparts, organelles are relatively stationary and motors are primarily implicated in the transport of vesicles [5], whose diffusion is negligibly slow [13]. A review of organelle movements in plant cells by Williamson [31] shows that movement of nearly all major organelles has been observed. Golgi stacks move over ER strands in an actomyosin-dependent manner [8,32], while the ER itself is also thought to bind to myosin motors [9,31,33,34]. There is also evidence for actomyosin-driven movement of mitochondria [35]. Chloroplasts are known to move along with streaming, as well as move themselves to positions determined by light and cell division planes, though the details of chloroplast–cytoskeleton contact are often less well understood [31].

### 1.4. Mixing in the cytoplasm

As Purcell famously outlined in his paper ‘Life at low Reynolds number’ [36], fluid flows at the cellular scale are dominated by viscosity, where our intuitions shaped by life in a high  $Re$  world do not apply. The Reynolds number  $Re = UL/\nu$  is the dimensionless ratio of inertial and viscous forces, containing a typical velocity  $U$ , a system size  $L$  and the kinematic viscosity  $\nu$  of the fluid. The properties of low Reynolds flows have important implications for mixing behaviour. A drop of milk in a glass of tea spreads in a turbulent cloud when stirred. As Taylor illustrated in his 1967 film ‘Low Reynolds number flows’ [37], this ‘mixing’ is reversible in a low  $Re$  flow. If a blob of dye is injected in a cylinder filled with a very viscous fluid, it apparently dissolves over a few turns of a stirrer, but if the stirrer’s motion is reversed the blob returns to its original shape, blurred only slightly by diffusion.

In considering diffusion of a solute of concentration  $c$  and diffusion constant  $D$  in the presence of a flow field  $\mathbf{u}$  we may rescale lengths by  $L$  and time by  $L^2/D$ , to obtain the dimensionless advection–diffusion equation

$$c_t + Pe(\mathbf{u} \cdot \nabla)c = \nabla^2 c, \quad (1.1)$$

where the Péclet number  $Pe = UL/D$  characterizes the relative strength of advection to diffusion in a form analogous to the Reynolds number. Small molecules in aqueous solutions have  $D \sim 10^{-5} \text{ cm}^2 \text{ s}^{-1} = 1000 \mu\text{m}^2 \text{ s}^{-1}$ . A  $1 \mu\text{m}$  bacterium, swimming at  $10 \mu\text{m s}^{-1}$ , would have  $Pe \sim 0.01$ . The smallest organisms therefore not only live in a world where the Reynolds number is essentially zero, they also live in a world where diffusive fluxes tend to outpace advective fluxes. Put more plainly: for a bacterium, it is equally efficient to sit in one place and let food arrive by diffusion as it is to swim to get it. Locomotion does not serve to increase uptake directly as much as it allows migration to areas richer in nutrients [36].

As the system size becomes larger, both  $Pe = UL/D$  and  $Re = UL/\nu$  increase, since they share a dependence on  $UL$ , but since  $D$  is typically three (or more) orders of magnitude smaller than  $\nu$ , the Péclet number becomes significant long before the Reynolds number does. By definition, advection competes with diffusion when  $Pe \sim 1$ , and this provides us with an estimate of the dimensions at which flow could

potentially aid cellular metabolism. For a typical length of  $10\ \mu\text{m}$  and a flow rate of  $1\ \mu\text{m s}^{-1}$ , structures with a diffusion constant lower than  $10\ \mu\text{m}^2\ \text{s}^{-1}$  will start to be affected by internal circulation. This number roughly corresponds to the diffusion rate of vesicles in the cytoplasm [13], indicating that active transport of vesicles may be worthwhile even in small cells. For small molecules, on the other hand, diffusion constants of order  $1000\ \mu\text{m}^2\ \text{s}^{-1}$  imply system sizes closer to  $100\ \mu\text{m}$  for transport rates in the range of  $10\ \mu\text{m s}^{-1}$ . So we see that active transport phenomena, which have typical velocities of  $1\text{--}10\ \mu\text{m s}^{-1}$ , could well be significant in aiding intracellular transport. However, in the absence of turbulent mixing, the precise mechanism by which transport is facilitated in the presence of a flow does need qualification. Some of the mechanisms by which flows may aid molecular transport at low Reynolds numbers are outlined below.

### 1.5. Chaotic flow fields

One mechanism often discussed for increasing diffusion and reaction rates involves chaotic advective fields, in which trajectories of neighbouring points diverge exponentially over time [38,39]. Mixing enhancement of this type has been studied extensively for microfluidic and lab-on-a-chip systems [40]. Examples include the herringbone micromixer, in which a chaotic circulation pattern is induced by a spatially alternating pattern of grooves in the bottom of a channel [41], and mixing in a droplet undergoing periodic deformations induced by electrowetting [42]. A pictorial way of describing these effects is that the surface described by the interface between two solutions is repeatedly stretched and folded into itself, much like the swirl of a Danish pastry, resulting in a drastic reduction of the length over which molecules have to diffuse.

### 1.6. Taylor dispersion

Another well-known mechanism of dispersion at low Reynolds numbers is *Taylor dispersion*, an enhancement of effective diffusivity due to shear that was originally described by G.I. Taylor in the context of pressure-driven pipe flows [43–45]. A layer of solute carried along by such a flow is deformed into a parabolic sheet by the velocity profile. This results in outward diffusion at the leading edge of the profile, and inward diffusion at the tail. After a time long enough for diffusion to smooth out the deformed sheet radially, it converges to a self-similar profile that travels with the mean flow speed and disperses with an effective diffusion constant

$$D_{\text{eff}} \simeq D \left( 1 + \frac{1}{192} Pe^2 \right), \quad (1.2)$$

which can greatly exceed the bare value  $D$ . In applying such concepts to subcellular mixing, it must be recognized that results obtained in long channels or many repeated drop deformations do not necessarily translate to the intermediate length and time scales found in single cells. As the time scale for diffusion across a channel of height  $h$  is  $h^2/D$ , whereas the distance travelled along the channel in this time is  $Uh^2/D = Peh$ , we should therefore expect the Taylor dispersion to become observable only when the aspect ratio  $L/h > Pe > \sqrt{192}$ .

### 1.7. High Péclet enhancement of reactive fluxes

An example of how advection can affect nutrient uptake was found in theoretical studies of the *Volvocales* [46,47]. These

algae take the form of spherical colonies that swim through their environment by the action of flagellated cells on their surface. The flow at the leading edge of the colony compresses a solute boundary layer closer to the surface of the cell, while a depleted plume is formed at the trailing edge. This effect produces a boundary layer whose size scales as  $Pe^{-1/2}$ , resulting in an enhanced concentration gradient and thereby an increased flux into the organism [46]. This flux enhancement is but one instance of a more general phenomenon. For *life at high Péclet numbers*, the boundary layers around metabolically active objects will shrink with increasing strength of the flow field, thereby facilitating increased fluxes into the object. Pickard [48] has recently applied these ideas to analysis of moving objects in the cytoplasm. Approximating vesicles and organelles as spherical objects he showed that the advective flux scales as  $Pe^2$  for  $Pe \lesssim 10$ , and crosses over to a  $Pe^{1/3}$  scaling for  $Pe \gtrsim 10$ . At  $Pe = 1$ , fluxes should be expected to be increased by roughly 100% over the purely diffusive value.

In summary, as a result of advances in fluorescence labeling techniques and biochemical knowledge over the past decades, we are now arriving at an understanding of the eukaryotic cytoplasm as a dynamic environment that is both crowded and highly structured, possessing tight homeostatic control mechanisms as well as a motor-driven infrastructure for precise routing of proteins towards their destination. It is increasingly becoming clear that quantitative understanding into trafficking and homeostatic control in this environment will require formulation of a spatially resolved picture of signalling and reaction rates along metabolic pathways.

Active transport processes mediated by molecular motors may play a key role in extending the spatial range over which metabolites can be reliably expected to interact, and it is in this context that the role of continuous forms of circulation observed in some larger cells is of interest. While the precise effect of advection on diffusive transport depends critically on the type of geometry studied, various mechanisms for enhancement of molecular transport can be identified for flows where the Péclet number is sufficiently large. The remainder of this review provides an overview of what is known about cytoplasmic streaming and its effect on intracellular transport. We pay particular attention to what is perhaps the best studied instance of this phenomenon, the *rotational streaming* that occurs in the giant *internodal* cells of the characean algae, but also indicate emerging areas of interest in other organisms.

## 2. Cytoplasmic streaming

Cytoplasmic streaming has been known for more than two centuries, with the first observations attributed to Bonaventura Corti in 1774 [49]. It occurs in a range of cell types and a variety of organisms, including amoebae, protozoa, fungi and slime moulds, and is also found during oogenesis in the fruit fly [50] and embryogenesis in the nematode *Caenorhabditis elegans* [51], though it is most common in plants and their highest genetic predecessors, the *characean algae* [1,52–55]. A large body of research over the last five decades has established that streaming is in most instances driven by an actomyosin system [56,57], but there are also examples of microtubule-based organelle movement [58–60]. Though the mechanics of cytoplasmic streaming have been studied extensively, there is relatively little insight into its biological function. A number of authors,

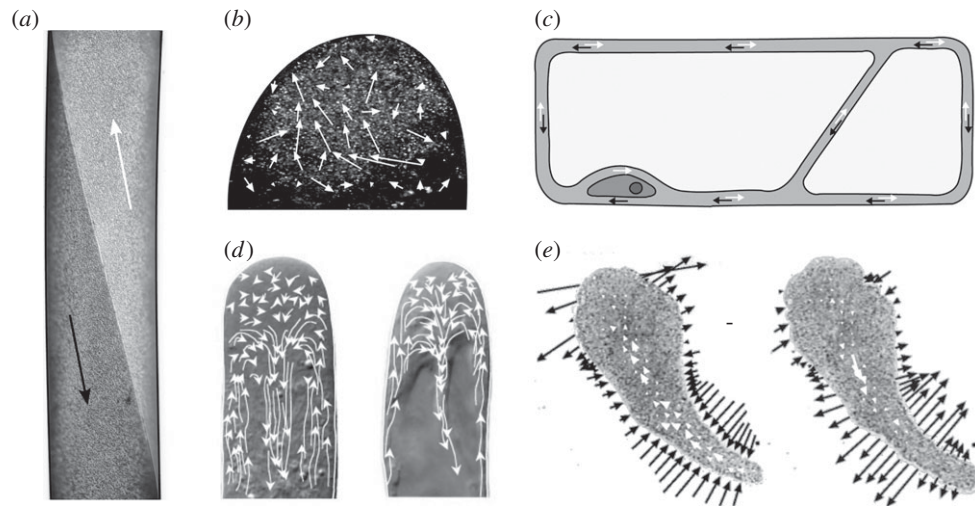


**Figure 2.** Topologies of cytoplasmic streaming. (a) Rotational streaming in internodal cells of *Chara corallina*. (b) A developing oocyte of *Drosophila* exhibits a correlated random flow field with typical flow rates of a few to tens of nanometres per second. Schematic of the velocity field, extracted by particle image velocimetry. (c) Circulation streaming in the periphery and transvacuolar strand of epidermal cells, e.g. as found in the root of *Medicago truncatula* [72]. (d) Reverse-fountain streaming in *Lilium longiflorum* (left) and *Nicotiana tabacum* (right). (Image modified from [73].) (e) Periodic shuttle streaming in plasmodium fragments of *Physarum polycephalum*. (Adapted from [63].)

most notably Pickard, have suggested that streaming may enhance metabolic rates in large cells, where diffusive time scales become prohibitively large [3,61,62].

Streaming has customarily been classified into two major groups. The term *amoeboid* streaming denotes cytoplasmic motion that induces changes in cell form, the best known of which is *shuttle streaming* found in slime moulds [52,54,55]. Non-amoeboid streaming is generally divided into five classes based on visually apparent phenomenology, as originally identified by Kamiya [1,52,62]. The best studied by far is the *rotational streaming* found in characeans, which will be reviewed in detail in the next section. Other forms of streaming commonly identified are *saltation*, *circulation*, *fountain streaming* and *multi-striate streaming*, briefly described later.

*Shuttle streaming* (figure 2e) is a periodic flow found in the *plasmodium* of slime moulds. The plasmodium is a single-celled aggregate of protoplasm containing many nuclei. As the organism searches for food, it forms a network of veins, known as *pseudopodia*, that self-optimizes in connecting to food sources and can find the shortest routes through mazes [64–66]. Rhythmic back-and-forth streaming of the cytoplasm takes place inside these filaments, driven by contraction waves in the actomyosin network. The velocities of this pressure-driven motion, which reverses every 2–3 min, can reach  $1350 \mu\text{m s}^{-1}$  [52].

*Random streaming* is a spatially correlated yet apparently unordered motion of the cytoplasm. The best-known example of this is found in various developmental stages of *Drosophila* [67–70]. There, within an oocyte several hundred micrometres across, kinesins moving along a dense network of microtubules producing streaming flows that vary from one oocyte to another, and over time within a given oocyte, and consists of swirls and eddies with a correlation length of some  $20 \mu\text{m}$  [50]. The nature of transport on such a disordered network is under active study [71].

*Saltation*, also known as *agitation*, is the most widespread form of cytoplasmic movement [1,52], characterized by apparently random jumps of cytoplasmic particles over distances as large as  $100 \mu\text{m}$ , much greater than those corresponding to thermal fluctuations. Microtubules are possibly implicated in this form of streaming, since very active saltation

is observed near spindles, within centrosomes and adjacent to microtubular organelles [1].

*Circulation* (figure 2c) takes the form of movement along the cell wall and strands of cytoplasm transecting the vacuole. Circulation patterns are typically stable on the time scale of minutes, and evolve as transvacuolar strands move and branch. Both unidirectional and bidirectional movement are known and velocities can be as large as  $40 \mu\text{m s}^{-1}$ . Cells exhibiting circulation include hair cells in various plants such as *Urtica* (stinging nettle), and parenchymal (i.e. bulk) cells in *Allium* (the onion genus), as well as the leaf cells of the water plant *Elodea* [1,52].

*Fountain streaming* (figure 2d) is circulation in which the cytoplasm moves along a central axis, flowing back in the opposite direction along the cell wall. *Reverse-fountain streaming* exhibits an inward motion along the central axis and is the more common of the two [1,53]. In some cell types, it is a developmental stage towards rotational streaming. True fountain streaming is typically found in root hairs and pollen tubes of various plants [72–80].

*Multi-striate streaming* is found in the fungus *Phycomyces* and in the marine alga *Acetabularia*. The cells of *Acetabularia* have a cylindrical stalk several centimetres in length, containing a large vacuole separated by a tonoplast from a thin layer of cytoplasm, at the periphery. Streaming occurs in both directions along channels separated by stationary cytoplasm [1]. Some forms of circulation could arguably be seen as multi-striate streaming, such in the marine alga *Caulerpa*, where streaming forms  $100 \mu\text{m}$  wide bands wherein files of chloroplasts stream bidirectionally in a circadian rhythm [1].

### 3. The characean algae

One of the most studied examples of cyclosis is the rotational streaming in giant cylindrical cells of the characean algae, or Charales (figure 3). Colloquially known as *stoneworts* after the lime deposits on their surface, these plant-like species are found in dense meadows on the bottom of lakes and ponds. *Chara* cells have been studied since the early days of microscopy

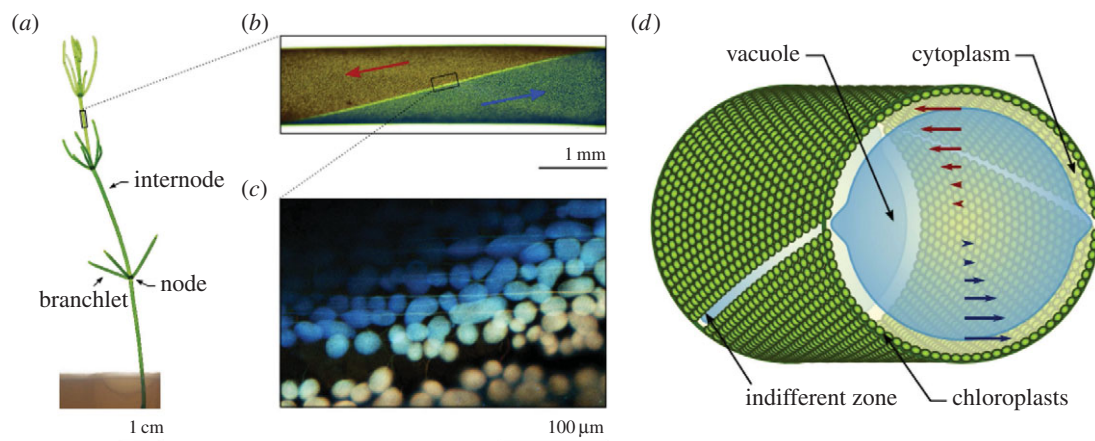


**Figure 3.** Rotational streaming in the characean algae. (a) A shoot of *Chara corallina* anchored in agar. Single-celled internodes connect nodal complexes where a whorl of six branchlets is formed. (b) Cytoplasmic streaming takes place along two domains shaped as spiralling bands. (c) This circulation is driven by the motion of myosin molecular motors along bundled actin filaments. This image shows a merged stack of confocal slices, with the colours denoting the focal position. Actin bundles can be observed below chloroplast rows at the surface of the cell. (Image courtesy S. Ganguly.) (d) The motion of myosin at the periphery entrains the outer layer of cytoplasm, which is of order  $10\ \mu\text{m}$  in thickness. The two moving bands are separated by a neutral line visible as a row of missing chloroplasts. The motion at the wall induces a shear flow in the central vacuole of the cell.

[49], and the species are now recognized as the closest living relatives of land plants [81,82]. This high degree of similarity, and the robustness of internodal cells under manipulation, has made them a model organism in a wide range of plant physiology research, including membrane transport and electrophysiology [83], turgor-driven cell wall expansion [84–90] and cytoskeletal organization [91–97], calcification and carbon fixation [98], intercellular transport through plasmodesmata [99–103] and even lake ecology [104–108].

Found in fresh and brackish waters, the characean algae have the appearance of plants, growing in thin segmented shoots that sprout whorls of branchlets every few centimetres (figure 3a). Their most studied part is the internode (figure 3b), a single cylindrical cell with a diameter up to 1 mm and a length that can exceed 10 cm. Like most plant cells, it is enclosed by a cellulose-containing cell wall, lined by a layer of *cytoplasm* approximately  $10\ \mu\text{m}$  in thickness. A membrane known as the *tonoplast* separates the cytoplasm from the central vacuole that occupies the bulk of the cell. This vacuole fulfils a multitude of metabolic roles, acting as storage compartment for sugars, polysaccharides and organic acids, sequestering toxins such as heavy metals, and functioning as a buffering reservoir that helps to maintain ionic and pH homeostasis in the cytoplasm [109]. Additionally, the vacuole holds a  $0.13\ \text{M}$  concentration of salts [110], producing a turgor pressure equivalent to 5 bar that lends the cell its rigidity.

The characean cytoplasm contains many structures that are common to higher plants, including the Golgi apparatus, ER and cytoskeletal filaments. *Chloroplasts*, the organelles responsible for photosynthesis, are packed into helical rows that spiral along the cell surface (figure 3d). The chloroplasts are surrounded by a stagnant layer of fluid, the *ectoplasm*, that houses most of the *mitochondria* in the cell [111]. On the inside of the chloroplast rows, bundled actin filaments (figure 3c) act as tracks for myosins that drag structures within the cell [34,112], and thereby entrain the inner part of the cytoplasm, the *endoplasm*. With streaming rates as high as  $100\ \mu\text{m s}^{-1}$ , the myosin XI found in *Chara* is the fastest known in existence [56]. As a result of a reversed polarity of the actin filaments, the cytoplasm is organized into two bands flowing in opposite directions. These bands spiral around each other, producing

a ‘barber-pole’ velocity at the cell periphery (figure 3c,d). The two interface lines between these bands are known as *neutral lines* or *indifferent zones*. They are marked by the absence of chloroplasts (figure 3d) and are visible as two light lines crossing the cell surface.

The internodes connect to the nodal structures by means of channels known as *plasmodesmata*. These channels are bridges of cytoplasm between cells. The plasmodesmata in Charales are similar to those found in higher plants, but may have evolved separately [101]. Most notably, in higher plants the ER is known to extend through plasmodesmata, but characean algae lack this feature. The generally accepted size limit for these channels is 800–1000 Da [113] for diffusive transport, though molecules as large as 45 kDa have been shown to move between cells on longer time scales [100].

### 3.1. Rate of streaming and velocity profile

The symmetry of characean internodes makes them amenable to a relatively straightforward hydrodynamic description. Internodal cells have a very large aspect ratio, typically exceeding 30, so, for positions sufficiently far from the endpoints, the flow is well approximated as that inside an infinite cylinder, with the cytoplasmic bands effectively imposing a value for the velocity at the boundaries (figure 4a). The Reynolds number  $Re = UR/\nu$  is at most 0.05, so the full hydrodynamic equations reduce to the linear *Stokes flow*, in which

$$\eta\nabla^2\mathbf{u} = \nabla p, \quad \nabla \cdot \mathbf{u} = 0. \quad (3.1)$$

Pickard [117] solved the simplest case of this flow problem for *Chara*, assuming straight, non-twisting indifferent zones lying along the  $z$ -axis. In this case, solving Stokes flow reduces to solving Laplace’s equation on a circle and the solution of the form  $u_z \sim \sum W^n r^n \sin(n\theta)$  is obtained readily by separation of variables. Assuming step boundary conditions (velocity  $\pm U$  on the two halves of the circle) allows a closed-form solution

$$u_z = \frac{2U}{\pi} \arctan\left(\frac{2(r/R)\sin\theta}{1 - (r/R)^2}\right). \quad (3.2)$$

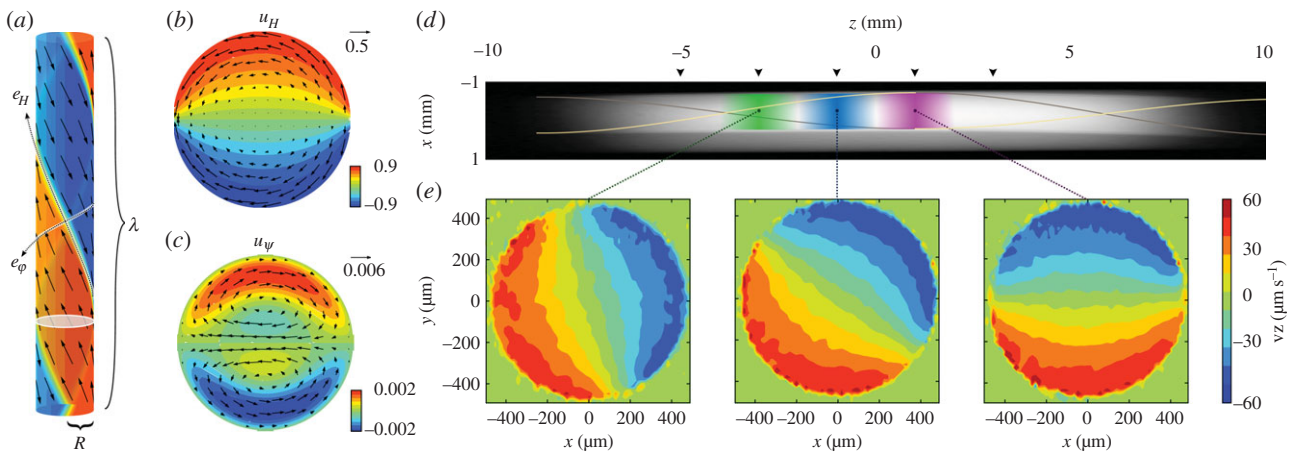


**Figure 4.** Hydrodynamic prediction and MRV measurements of vacuolar flow. (a) The internodal flow has a helical symmetry: an invariance under a translation along the longitudinal axis combined with a rotation. The two axes that naturally follow from this symmetry are the vector  $e_H$ , which points along the bands, and the vector  $e_\phi$ , which is orthogonal to the bands. (b) Theoretically predicted flow field along the  $e_H$  component, showing the vacuolar shear profile. (c) The  $e_H$  and  $e_\phi$  components reveal a small secondary circulation along the centre of the cell. (d) MRI scan of an internode placed in a glass tube, with spiralling lines indicating positions of the neutral line, and coloured bands showing the domains used for velocity measurements. (e) Velocity profiles measured at each of the domains show excellent agreement with the theoretical profile. (Figures modified from [114–116].)

A general solution for the case of twisting helical bands of wavelength  $\lambda$  can be obtained as Fourier–Bessel series [114,115]. A decomposition along the axis of symmetry (figure 4a) shows that the flow field possesses two components, a downstream term that reduces to the profile (3.2) in the limit of infinite helical pitch, and a small-amplitude circulation between the neutral lines. The amplitude of the second term vanishes as  $\lambda \rightarrow 0$  and  $\lambda \rightarrow \infty$ , reaching a maximum for  $\lambda/R \sim 3$ . During development of the internodes, the helical bands twist and subsequently untwist, attaining a minimum in the helical pitch roughly at the stage of maximal growth [118]. It is therefore possible that this secondary circulation, though modest in amplitude, aids homeostasis by enhancing vacuolar mixing [114,115].

A series of increasingly sophisticated experiments, employing first visual tracking [117,119] and later laser Doppler spectroscopy [120], has shown that the approximation of a simple shear flow is in good agreement with the *in vivo* observations. Recently, full two-dimensional measurements of the velocity field were obtained using magnetic resonance velocimetry (MRV) (figure 4c,d), which confirm that the vacuolar flow is virtually indistinguishable from its hydrodynamic prediction [116], with direct shear transmission by the tonoplast. The role of a lipid membrane in allowing such direct shear transmission has recently been investigated theoretically [121] and experimentally [122].

### 3.2. Cell development

In order to extend towards sunlight, plant cells expand their volume 10–20-fold over the course of development [86,109]. The majority of this volume is occupied by the central vacuole, where high concentrations of salts are sequestered, resulting in large outward osmotic pressures that maintain the rigidity, or *turgor*, of the cell. Perhaps one of the most important functions of these vacuolar balloons is to serve as an energetically favourable means of expanding the volume of the organism. While there is a considerable cost associated with the transport against electrochemical gradients required to maintain the solute concentration in the vacuole, it is much cheaper to expand cell size by water uptake than by protein

synthesis [109,123]. With their exceptionally long internodal cells, whose vacuoles occupy about 95% of the cellular volume, characean algae represent an extreme case of this growth strategy. Since these species grow as weeds in low-nutrient conditions and can outcompete higher plants for lake dominance [124], the large cell size in these organisms may be partially understood as a result of competition for light in low-nutrient conditions.

Growth in characean algae occurs by repeated division of a single cell at the plant tip, the *apical cone* [125]. During shoot development, this cell divides every few days. The rate of this division, sometimes called the *plastrochron*, can be quite regular. After division, the newly formed cell divides once more into an upper *pro-node* and an internode. The internode undergoes a remarkable degree of expansion, increasing in volume by five orders of magnitude during two to three weeks [125]. The pro-node undergoes a number of subsequent divisions to form the nodal structure. In *Chara corallina*, there is an initial division into six cells which connect to the ascending and descending streams in a specific manner [126]. In later stages, these cells undergo further divisions to form a complex multicellular structure, though the initial symmetry is still reflected in the fact that *C. corallina* typically forms a whorl of six branchlets. The reproductive structures are exclusively formed on the part of the node connecting to the descending stream [126].

### 3.3. Nutrient uptake and intercellular transport

One of the most obvious roles of cytoplasmic streaming in characean metabolism is to enhance the rate of transport between cells, thereby facilitating the translocation of nutrients from regions of uptake to regions of growth. Because of their relative anatomical simplicity, the Charales have been used for a great number of uptake and transport studies using radioisotopes to track salts [127–130] and nutrients such as inorganic carbon [99,128–131], nitrogen and phosphorus [132–135].

Like most aquatic macrophytes, the Charales are able to take up nutrients from the surrounding water, in contrast to land plants where uptake predominantly takes place in the roots. While the species can successfully be cultured in

flasks without needing to be anchored in a layer of soil [136], there is evidence that a significant proportion of uptake may take place in the root-like *rhizoidal* cells that anchor the plants, particularly for rate-limiting nutrients such as phosphorus and nitrogen which may be more abundant by orders of magnitude in the interstitial water of the sediment [132–135].

Dissolved inorganic carbon (DIC) is taken up directly from the water surrounding the shoot. Low-weight carbohydrates are formed within 1 h after uptake of  $^{14}\text{C}$ -DIC and pass unaltered through the plasmodesmata to the neighbouring cell [131]. The bulk of the photoassimilates reside in the endoplasmic layer on the inside of the chloroplasts, but particularly in branchlet cells some fraction is sequestered in the vacuole [137]. The branchlet cells are more photosynthetically active than the internodes, and transport from the branchlets to internodes can be five times higher than the reverse [137,138].

Many studies have investigated the relationship between streaming and intercellular transport. Measurements with a tandem pair of internodes show that the transport rate correlates with the streaming rate over the 25% variation in magnitude observed in a collection of samples [129]. This correlation is stronger in summer when the rate of transport is higher [126,129,139]. Treatment with cytochalasin B shows a roughly proportional reduction of the transport rate with the streaming velocity [140]. Treatment of either cell in the pair suffices to lower the transport rate; a similar response is found when altering the streaming velocity by lowering the temperature [99]. Some early studies found indications of a small component of propagation faster than the streaming velocity [128,141], but this finding was not confirmed by later whole-shoot experiments where  $^{14}\text{C}$  is fed to the rhizoids, showing that carbon is transported upwards at roughly the rate of streaming while  $^{32}\text{P}$  transport is somewhat slower [142].

### 3.4. Alkaline band formation and carbon fixation

The lime deposits from which the species get the name *stoneworts* arise from their alkaline habitat. Carbon fixation associated with photosynthesis naturally leads to production of  $\text{OH}^-$ , as can be seen in the pH dependence of the chemical equilibrium of DIC in water



At pH 5.5 roughly 90% of the dissolved carbon is found in the form  $\text{CO}_2$ , but as the pH increases this balance shifts towards  $\text{HCO}_3^-$ . At pH 8.5, which is fairly typical for environments inhabited by characeans, 99% of the inorganic carbon is in  $\text{HCO}_3^-$ . A proton is therefore required to produce  $\text{CO}_2$  from bicarbonate, which inevitably leaves  $\text{OH}^-$  as a side product. This excess  $\text{OH}^-$  is excreted at the surface, inducing a rise in pH. In characeans  $\text{OH}^-$  is localized in periodically spaced alkaline bands alternated by acidic regions where  $\text{H}^+$  efflux occurs [143]. Calcium carbonate ( $\text{CaCO}_3$ ) tends to precipitate on the alkaline regions forming the band-shaped encrustations characteristic of stoneworts. This precipitation yields a proton,



which may then be used to produce  $\text{CO}_2$  from bicarbonate. It has been suggested that the  $\text{H}^+$  efflux serves to facilitate photosynthesis by raising the concentration of free  $\text{CO}_2$  [144]. Evidence that this precipitation enhances carbon fixation is found in  $^{14}\text{C}$  studies that show a 1 : 1 correspondence between

the rate of  $\text{CaCO}_3$  precipitation and the rate of carbon fixation in slightly alkaline environments of pH 8–9 [145–147].

Further support for the notion the pH bands enhance photosynthesis is found in the work by Mimura *et al.* [148], who investigated the effect of the  $\text{H}^+$ -ATPase on  $^{14}\text{C}$  fixation. They observed that carbon fixation was strongly reduced both when the ATP in the cytoplasm was depleted by perfusion with hexokinase and 2-deoxyglucose and when the  $\text{H}^+$ -ATPase was inhibited by introduction of vanadate. Stimulation of the  $\text{H}^+$ -ATPase by pyruvate kinase and phosphoenolpyruvate (PEP) resulted in increased carbon fixation. The same effects were observed at both pH 5.5 and pH 8.5, indicating that the  $\text{H}^+$ -ATPase plays an essential role in assimilation of both  $\text{CO}_2$  and  $\text{HCO}_3^-$ . Evidence that the formation of alkaline bands directly influences the rate of photosynthesis is also found in *fluorometry* studies. When a sample is excited with light, the absorbed light can be used for photosynthesis, emitted as fluorescence or dissipated as heat. In practice, the degree of heat dissipation can often be taken as constant, so the fluorescence signal represents an inverse measure of the rate of photosynthetic activity. Such measurements show that the external pH correlates directly with the rate of photosynthetic activity, with the highest rates observed in acidic regions [149,150].

Alkaline band formation appears inseparably linked to cytoplasmic streaming. The magnitude of pH variations is greater for the upwards streaming band than for the downwards streaming band [151], and inhibition of cytoplasmic streaming with cytochalasin B prevents formation of alkaline bands [143,152]. The membrane of internodal cells can undergo an *action potential*, a transient depolarization similar to that observed in nerve cells, although the travel speed of about  $1 \text{ cm s}^{-1}$  is much slower. During an action potential, streaming is momentarily halted and the alkaline bands disappear. As streaming recovers, the alkaline bands tend to reform at the same position on the cell's surface and the recurrence was increased with the concentration of  $\text{Ca}^{2+}$  in the surrounding medium [153].

Although models for the formation of alkaline bands have been presented [154], the specific role of streaming in the generation of alkaline bands has not been widely discussed in the literature. A function of streaming thus far overlooked may well be to drive these bands, thereby aiding carbon uptake from the environment and enhancing photosynthetic rates.

### 3.5. Driving mechanics and cytoplasmic rheology

Various studies have investigated the driving mechanism and rheological aspects of cytoplasmic streaming. A number of authors have presented theoretical models of transport along the cytoskeleton with stochastic on–off dynamics [155–158]. The most recent work of this form applied to streaming is by Houtman *et al.* [159], who describe streaming in transvacuolar strands with a two-dimensional model that includes on/off kinetics and hydrodynamic interactions between particles through the Oseen tensor. There is also a range of studies that focus on the driving force associated with streaming. Pickard [61] investigated the scaling of streaming with cell size, presenting an analysis to support the notion that most dissipation occurs near the neutral lines. His measurements of the streaming velocity as a function of cell size show the scaling of the maximum streaming speed  $U \sim R^{1/2}$ , which is consistent with the combined assumption of a dissipation rate scaling as  $U^2$  and a driving power scaling as  $R$ .

Tazawa & Kishimoto [160] measured the motive force using perfusion experiments. In this technique, the cell is placed in an isotonic bath (i.e. a solution of an osmolarity similar to that of the vacuolar fluid), which allows the cell to survive amputation of its ends. If each of the endpoints is then contained in a compartment separated from the rest of the bath, the contents of the vacuole can be replaced by applying a slight pressure difference [110,161]. To measure the motive force, the pressure difference between the two reservoirs is adjusted so that streaming is halted in one of the bands, implying that the shear force balances the motive force in the cytoplasmic layer. The motive force obtained this way has a value in the range of 14–20  $\mu\text{N cm}^{-2}$ , consistent with centrifuge microscope measurements [162]. Of note here is that this force is independent of temperature. Rates of cytoplasmic streaming show a widely documented linear (or even exponential) dependence on temperature [52,61,163,164], with Pickard [61] reporting an increase of 3.4  $\mu\text{m s}^{-1} \text{K}^{-1}$ . Tazawa's results therefore suggest that this temperature dependence is a consequence of a change in cytoplasmic viscosity. Tazawa & Kishimoto also examined the effect of tonicity, finding that an increase in the tonicity from 290 to 586 mM results in a lowered streaming rate as well as an increased motive force. Decreasing the tonicity in the cytoplasm to 190 mM resulted in a swelling of the chloroplasts, causing a marked decrease in streaming rate and motive force, presumably because of a resulting deformation in the actin bundles. After 5–20 min, the chloroplasts regained their normal shape and streaming recovered, though the motive force remained lowered.

Donaldson [165] performed measurements of the forward streaming velocity as a function of the applied perfusion pressure gradient. He assumed a driving force localized to a layer of thickness  $\epsilon$  and a power-law dependence  $\tau = -\alpha(\partial u/\partial y)^{1/n}$  for the viscous stress. His results show a good correspondence for  $n=3$  and  $\epsilon=0.1 \mu\text{m}$ . The corresponding motive force,  $F=36 \mu\text{N cm}^{-2}$ , is higher than the values found by others [160,162], which he concludes is the result of a systematic underestimation in those measurements due to the fact that the small velocities and thin layers of movement near the stalling point are very difficult to observe. Hayashi [166] applied a similar analysis to experimentally measured velocity profiles. Like Donaldson he assumed a power-law rheology and found the best-fit parameters for measurements of a protoplasm-filled cell [119], as well as two cases of plug flow of extracted cytoplasm [167]. He found an exponent of  $n=1.4$  for the protoplasm-filled cell and exponents of  $n=1.3$  and  $n=1.7$  for two cases of plug flow.

Nothnagel & Webb [168] investigated various hydrodynamic models for driving mechanics in the cytoplasm and concluded that the virtually shear-less profile observed in the cytoplasm is best explained by assuming a meshwork throughout the cytoplasm that is pulled along at the cell wall. The ER is argued to be a structure that could fulfil such a role, and there is structural evidence from electron micrographs to support this hypothesis [34]. Recent work [169] has examined the importance of hydrodynamic slip at the cell wall.

#### 4. Role in intracellular transport

Although a great deal of work has been published on the molecular basis and hydrodynamics of streaming, relatively

few authors venture into a discussion of its function. It has long been suggested that streaming aids molecular transport in some way. Kamiya's 1959 review [52] mentions that de Vries suggested this as early as 1885 [170]. However, concrete hypotheses as to the mechanism by which streaming accelerates metabolic rates have scarcely been put forward. Agutter *et al.* [11,12] have argued that diffusion is not capable of explaining many transport phenomena in cells. Similarly, Hochachka [3] presents an argument that the degree of homeostasis along ATP pathways cannot be explained other than by assuming forms of active transport.

The highly symmetric topology of streaming in the characean algae would appear to have evolved at considerable evolutionary cost, as further reflected in the fact that the myosin XI found in this organism is the fastest known in existence. On the basis of what we know about the characean algae, we see that streaming is implicated in a multitude of roles in cellular metabolism. It aids transport between cells and is therefore essential in supplying a steady flow of cellular building blocks to newly formed cells at the tip of the shoot. It also appears important in maintaining the alkaline bands that facilitate uptake of inorganic carbon from the surrounding water. However, a key question that remains largely unanswered is just what role streaming may play in eliminating the diffusional bottlenecks that would seem to limit cell sizes in other organisms. Indeed, streaming may help homeostatic regulation during rapid cell volume expansion, but the precise mechanisms by which it does so remain an open area of investigation.

The most important contributions in terms of a quantified discussion of the effect of streaming on intracellular transport are without doubt from Pickard. He discussed scaling of the streaming velocity and diffusional time scales with cell size [61], as well as the interaction between the stagnant layer of periplasm surrounding the chloroplast rows, and the moving layer of endoplasm. He points out the possibility that advection of a point-source may aid homeostasis by smoothing out fluctuations in the concentration field. He also raises the notion that streaming as such does not necessarily have to confer a benefit to the cell if its real purpose is transport of particles along the cytoskeleton. This second point is argued further in a later publication where he makes a case for streaming being an accidental consequence for vesicular transport along the cytoskeleton [62]. As covered in §1.4, he also discusses the role of boundary layer scaling in enhancing exchange of molecular species between organelles and their environment in advection-dominated flows [48].

Our own work on the secondary circulation in the vacuole mirrors this last theme of life at high Péclet numbers [114,115]. In the case of a cell with helically twisted bands, the secondary circulation vortices in figure 4c produce an advection from centre to wall and vice versa. In the case of a transient uptake into the vacuole, this produces a boundary layer at the left side of the cross section, where the flow is directed outward, while diffusional pile-up is carried inward at the opposite neutral line. The boundary layer arising from this effect scales as  $Pe^{-1/3}$ . This phenomenon suggests that the helicity of the bands, which is maximized at the moment of greatest growth, may serve to aid cellular homeostasis by facilitating enhanced diffusive fluxes into and out of the vacuole, allowing it to play a buffering role with respect to metabolic processes in the cytoplasm. However, analysis of the eigenmodes of transient decay towards a well-mixed vacuolar concentration



**Figure 5.** Self-organization of cytoplasmic streaming in a mathematical model of *Chara* [174]. Colour coding corresponds to the  $z$ -component of an order parameter associated with actin filaments at the periphery, and white lines represent indifferent zones separating up- and down-streaming regions. Superimposed are streamlines of the cytoplasmic flow induced by the filament field, where the flow is directed from the thin end to the thick end of the individual lines. Panels show progression from random disorder through local order to complete steady cytosol.

shows that the enhancement of fluxes into and out of the vacuole would become significant from  $Pe_\psi \gtrsim 10$ . This suggests that this type of effect would primarily benefit transport of slowly diffusing structures, such as large macromolecules, whose presence in characean vacuoles has currently not been established [171].

## 5. Streaming and cell size: key questions

As emphasized in the mini-reviews in the above sections, the past two decades have led to remarkable progress in our understanding of the biochemical pathways central to cellular metabolism. In terms of the dynamical behaviour of these systems, we have seen that there are two central challenges in cellular regulation. (i) Maintaining homeostatic levels of small molecules and ions across varying levels of metabolic turnover and (ii) the routing of proteins and other macromolecule intermediates towards their intended targets.

A fundamental question from a biophysical point of view is what constraints have governed the evolution of homeostatic control mechanisms and macromolecular targeting. It is clear that both these tasks are complex and will lead to requirements that vary between cell types and species. Yet while there are important differences, the functioning of the ER and Golgi complexes shows a high degree of similarity across a wide range eukaryotic species. The vesicle transport system in particular has been shown to be highly conserved, exhibiting essentially the same mechanisms in organisms as diverse as mammals and yeast [7].

Two basic questions any physicist will be inclined to ask are what typical length and time scales govern intracellular transport. This returns us to our initial question regarding the evolution of cell size to a typical range of 1–100  $\mu\text{m}$ . Presumably mechanisms for protein targeting and homeostatic control will be under increasing strain as the cell size increases. What, then, are the rate-limiting factors in these processes, and how is it that cells may be able to mitigate these limitations by internal circulation?

The internodes of characean algae present one of the most compelling test cases for these questions. Not only are these cells among the largest in Nature, but the form of streaming

found in this system is also the most organized and symmetrical of all types of circulation currently known. This means that the system is amenable to analysis from a geometrical point of view, and the many physiological studies performed on this organism mean that theoretical results can be placed in the context of detailed biological knowledge. Moreover, the fact that internodes grow from some 20  $\mu\text{m}$  to several centimetres provides an opportunity to study mechanisms of metabolic control at a range of scales.

One of the aspects of streaming in the characean algae that has yet to be elucidated is just how it affects transport of small molecules and vesicles in the cytoplasm. To the precision of current experimental techniques, the cytoplasm appears to move as a gelled layer, retaining its shape perhaps by way of the meshwork of ER tubes that extend throughout the endoplasmic compartment. The temporal and spatial variations in the velocity field have yet to be quantified. Given the typical velocities around 50  $\mu\text{m s}^{-1}$ , even the magnitude of relatively small fluctuations could be significant, particularly when it comes to the reported caged diffusion of vesicles.

Another physical issue for which deeper understanding is needed is the precise relation between the topology of the cytoskeletal network and the cytoplasmic flow. It would appear that streaming presents itself in increasingly organized forms as the system size is scaled up. This could be the result of evolutionary pressure, but could also be a physical effect. So given an actin network, a cytoplasmic rheology and the force–velocity relations of molecular motors, can we predict in what types of systems we will see continuous forms of circulation?

This leads us finally to comment on the possibility that some forms of streaming appear through a process of self-organization. As long ago as 1953 [172], it was noted that cytoplasmic droplets extracted from characean algae could spontaneously self-organize into rotating fluid bodies. This presumably arises from myosin motors that walk along dislodged actin filaments and entrain fluid. Each of these motor/filament assemblies constitutes a force dipole in the fluid, and nearby assemblies will be attracted together if nearly parallel, leading to self-reinforcement of local order, leading eventually to long-range order. Further evidence for

self-organization comes from much more recent work [173] in which steaming is completely disrupted through added chemicals (cytochalasin and oryzalin), which, when removed, allow streaming to be reconstituted. Strikingly, the indifferent zone appears in a new location. A mathematical model [174] that combines filament bundling, flow-induced reorientation and coupling to the curvature of the cell wall successfully reproduces much of this phenomenology, as shown in figure 5.

The hypothesis that streaming can self-organize through physical processes associated with hydrodynamic interactions arising from force dipoles leads naturally to the field of ‘active matter’, and in particular to the properties of

bacterial suspensions. Each bacterium can be thought of as a force dipole, with one force directed backwards from the trailing flagella and a second directed forwards from the action of the cell body on the fluid. The attractive interactions between such ‘pusher’ dipoles mentioned above has also been predicted to lead to simple large-scale flow topologies in bacterial suspensions [175], which has subsequently been verified [176,177].

**Funding statement.** This work was supported in part by the Leverhulme Trust, ERC Advanced Investigator grant no. 247333 and the Schlumberger Chair Fund.

## References

- Allen NS, Allen RD. 1978 Cytoplasmic streaming in green plants. *Annu. Rev. Biophys. Biol.* **7**, 497–526. (doi:10.1146/annurev.bb.07.060178.002433)
- Cannon WB. 1932 *The wisdom of the body*. New York, NY: WW. Norton & Co., Inc.
- Hochachka PW. 1999 The metabolic implications of intracellular circulation. *Proc. Natl Acad. Sci. USA* **96**, 12 233–12 239. (doi:10.1073/pnas.96.22.12233)
- Boller T, Wiemken A. 1986 Dynamics of vacuolar compartmentation. *Annu. Rev. Plant Physiol.* **37**, 137–164. (doi:10.1146/annurev.pp.37.060186.001033)
- Schwartz AL. 1990 Cell biology of intracellular protein trafficking. *Annu. Rev. Immunol.* **8**, 195–229. (doi:10.1146/annurev.iy.08.040190.001211)
- Chrispeels MJ. 1991 Sorting of proteins in the secretory system. *Annu. Rev. Plant Physiol. Plant Mol. Biol.* **42**, 21–53. (doi:10.1146/annurev.pp.42.060191.000321)
- Staehelin LA, Moore I. 1995 The plant Golgi apparatus: structure, functional organization and trafficking mechanisms. *Annu. Rev. Plant Physiol. Plant Mol. Biol.* **46**, 261–288. (doi:10.1146/annurev.pp.46.060195.001401)
- Jurgens G. 2004 Membrane trafficking in plants. *Annu. Rev. Cell. Dev. Biol.* **20**, 481–504. (doi:10.1146/annurev.cellbio.20.082503.103057)
- Staehelin LA. 1997 The plant ER: a dynamic organelle composed of a large number of discrete functional domains. *Plant J.* **11**, 1151–1165. (doi:10.1046/j.1365-313X.1997.11061151.x)
- Dupree P, Sherrier DJ. 1998 The plant Golgi apparatus. *Biochim. Biophys. Acta* **1404**, 259–270. (doi:10.1016/S0167-4889(98) 00061-5)
- Agutter PS, Malone PC, Wheatley DN. 2000 Diffusion theory in biology: a relic of mechanistic materialism. *J. Hist. Biol.* **33**, 71–111. (doi:10.1023/A:1004745516972)
- Agutter PS, Wheatley DN. 2000 Random walks and cell size. *Bioessays* **22**, 1018–1023. (doi:10.1002/1521-1878(200011)22:11<1018::AID-BIES8>3.0.CO;2-Y)
- Luby-Phelps K. 1999 Cytoarchitecture and physical properties of cytoplasm: volume, viscosity, diffusion, intracellular surface area. *Int. Rev. Cytol.* **192**, 189–221. (doi:10.1016/S0074-7696(08)60527-6)
- Alberts B, Johnson A, Lewis J, Raff M, Roberts K, Walter P. 2002 *Molecular biology of the cell*, 4th edn. New York, NY: Garland Science.
- Ellis RJ. 2001 Macromolecular crowding: obvious but underappreciated. *Trends Biochem. Sci.* **26**, 597–604. (doi:10.1016/S0968-0004(01)01938-7)
- Zimmerman SB, Minton AP. 1993 Macromolecular crowding: biochemical, biophysical, and physiological consequences. *Annu. Rev. Biophys. Biomol. Struct.* **22**, 27–65. (doi:10.1146/annurev.bb.22.060193.000331)
- Minton A. 1997 Influence of excluded volume upon macromolecular structure and associations in ‘crowded’ media. *Curr. Opin. Biotech.* **8**, 65–69. (doi:10.1016/S0958-1669(97)80159-0)
- Goodsell DS. 2009 *The machinery of life*, 2nd edn. New York, NY: Springer.
- Clegg JS. 1984 Properties and metabolism of the aqueous cytoplasm and its boundaries. *Am. J. Physiol.* **246**, R133–R151.
- Rorschach HE, Lin C, Hazlewood CF. 1991 Diffusion of water in biological tissues. *Scanning Microsc.* **5**, 1–10.
- Cameron IL, Kanal KM, Keener CR, Fullerton GD. 1997 A mechanistic view of the non-ideal osmotic and motional behavior of intracellular water. *Cell Biol. Int.* **21**, 99–113. (doi:10.1006/cbir.1996.0123)
- Verkman AS. 2002 Solute and macromolecule diffusion in cellular aqueous compartments. *Trends Biochem. Sci.* **27**, 27–33. (doi:10.1016/S0968-0004(01)02003-5)
- Luby-Phelps K, Taylor DL, Lanni F. 1986 Probing the structure of cytoplasm. *J. Cell Biol.* **102**, 2015–2022. (doi:10.1083/jcb.102.6.2015)
- Luby-Phelps K, Castle PE, Taylor DL, Lanni F. 1987 Hindered diffusion of inert tracer particles in the cytoplasm of mouse 3T3 cells. *Proc. Natl Acad. Sci. USA* **84**, 4910–4913. (doi:10.1073/pnas.84.14.4910)
- Popov S, Poo MM. 1992 Diffusional transport of macromolecules in developing nerve processes. *J. Neurosci.* **12**, 77–85.
- Arrio-Dupont M, Cribier S, Foucault G, Devaux P, Dalbis A. 1996 Diffusion of fluorescently labeled macromolecules in cultured muscle cells. *Biophys. J.* **70**, 2327–2332. (doi:10.1016/S0006-3495(96) 79798-9)
- Wachsmuth M, Waldeck W, Langowski J. 2000 Anomalous diffusion of fluorescent probes inside living cell nuclei investigated by spatially-resolved fluorescence correlation spectroscopy. *J. Mol. Biol.* **298**, 677–689. (doi:10.1006/jmbi.2000.3692)
- Weiss M, Elsner M, Kartberg F, Nilsson T. 2004 Anomalous subdiffusion is a measure for cytoplasmic crowding in living cells. *Biophys. J.* **87**, 3518–3524. (doi:10.1529/biophysj.104.044263)
- Banks DS, Fradin C. 2005 Anomalous diffusion of proteins due to molecular crowding. *Biophys. J.* **89**, 2960–2971. (doi:10.1529/biophysj.104.051078)
- Golding I, Cox EC. 2006 Physical nature of bacterial cytoplasm. *Phys. Rev. Lett.* **96**, 098102. (doi:10.1103/PhysRevLett.96.098102)
- Williamson RE. 1993 Organelle movements. *Annu. Rev. Plant Physiol. Plant Mol. Biol.* **44**, 181–202. (doi:10.1146/annurev.pp.44.060193.001145)
- Boevink P, Oparka K, Santa Cruz S, Martin B, Betteridge A, Hawes C. 1998 Stacks on tracks: the plant Golgi apparatus traffics on an actin/ER network. *Plant J.* **15**, 441–447. (doi:10.1046/j.1365-313X.1998.00208.x)
- Du Y, Ferro-Novick S, Novick P. 2004 Dynamics and inheritance of the endoplasmic reticulum. *J. Cell. Sci.* **117**, 2871–2878. (doi:10.1242/jcs.01286)
- Kachar B. 1985 Direct visualization of organelle movement along actin filaments dissociated from Characean algae. *Science* **227**, 1355–1357. (doi:10.1126/science.4038817)
- Van Gestel K, Köhler RH, Verbelen J-P. 2002 Plant mitochondria move on F-actin, but their positioning in the cortical cytoplasm depends on both F-actin and microtubules. *J. Exp. Bot.* **53**, 659–667. (doi:10.1093/jexbot/53.369.659)
- Purcell EM. 1977 Life at low Reynolds number. *Am. J. Phys.* **45**, 3–11. (doi:10.1119/1.10903)
- Taylor GI. 1966 *Low Reynolds number flow*. See <http://web.mit.edu/hml/nctmf.html>.

38. Aref H. 1984 Stirring by chaotic advection. *J. Fluid Mech.* **143**, 1–21. (doi:10.1017/S0022112084001233)
39. Aref H. 2002 The development of chaotic advection. *Phys. Fluids* **14**, 1315–1325. (doi:10.1063/1.1458932)
40. Squires TM, Quake S. 2005 Microfluidics: fluid physics at the nanoliter scale. *Rev. Mod. Phys.* **77**, 977–1026. (doi:10.1103/RevModPhys.77.977)
41. Stroock AD, Dertinger SKW, Ajdari A, Stone HA, Mezic I, Whitesides GM. 2002 Chaotic mixer for microchannels. *Science* **295**, 647–651. (doi:10.1126/science.1066238)
42. Mugele F, Baret J-C, Steinhauser D. 2006 Microfluidic mixing through electrowetting induced droplet oscillations. *Appl. Phys. Lett.* **88**, 204106. (doi:10.1063/1.2204831)
43. Taylor GI. 1953 Dispersion of soluble matter in solvent flowing slowly through a tube. *Proc. R. Soc. Lond. A* **219**, 186–203. (doi:10.1098/rspa.1953.0139)
44. Taylor GI. 1954 Conditions under which dispersion of a solute in a stream of solvent can be used to measure molecular diffusion. *Proc. R. Soc. Lond. A* **225**, 473–477. (doi:10.1098/rspa.1954.0216)
45. Taylor GI. 1954 Diffusion and mass transport in tubes. *Proc. R. Soc. Lond. B* **67**, 857–869. (doi:10.1088/0370-1301/67/12/301)
46. Short MB, Solari CA, Ganguly S, Powers TR, Kessler JO, Goldstein RE. 2006 Flows driven by flagella of multicellular organisms enhance long-range molecular transport. *Proc. Natl Acad. Sci. USA* **103**, 8315–8319. (doi:10.1073/pnas.0600566103)
47. Solari CA, Ganguly S, Kessler JO, Michod RE, Goldstein RE. 2006 Multicellularity and the functional interdependence of motility and molecular transport. *Proc. Natl Acad. Sci. USA* **103**, 1353–1358. (doi:10.1073/pnas.0503810103)
48. Pickard WF. 2006 Absorption by a moving spherical organelle in a heterogeneous cytoplasm: implications for the role of trafficking in a symplast. *J. Theor. Biol.* **240**, 288–301. (doi:10.1016/j.jtbi.2005.09.008)
49. Corti B. 1774 *Osservazione Microscopiche sulla Tremella e sulla Circolazione del Fluido in Una Planta Acquaguola*. Lucca, Italy: Appresso Giuseppe Rocchi.
50. Ganguly S, Williams LS, Palacios IM, Goldstein RE. 2012 Cytoplasmic streaming in *Drosophila* oocytes varies with kinesin activity and correlates with the microtubule cytoskeleton architecture. *Proc. Natl Acad. Sci. USA* **109**, 15 109–15 114. (doi:10.1073/pnas.1203575109)
51. Shinar T, Mana M, Piano F, Shelley MJ. 2011 A model of cytoplasmically driven microtubule-based motion in the single-celled *Caenorhabditis elegans* embryo. *Proc. Natl Acad. Sci. USA* **108**, 10 508–10 513. (doi:10.1073/pnas.1017369108)
52. Kamiya N. 1959 *Protoplasmatologia*. Vol. 8/3a. *Protoplasmic streaming*. Vienna, Austria: Springer.
53. Kamiya N. 1962 Protoplasmic streaming. In *Encyclopedia of plant physiology*, vol. XVII, pp. 979–1035. Berlin, Germany: Springer.
54. Kamiya N. 1981 Physical and chemical basis of cytoplasmic streaming. *Annu. Rev. Plant Physiol.* **32**, 205–236. (doi:10.1146/annurev.pp.32.060181.001225)
55. Allen RE, Allen NS. 1978 Cytoplasmic streaming in amoeboid movement. *Annu. Rev. Biophys. Biol.* **7**, 469–495. (doi:10.1146/annurev.bb.07.060178.002345)
56. Shimmen T, Yokota E. 2004 Cytoplasmic streaming in plants. *Curr. Opin Cell Biol.* **16**, 68–72. (doi:10.1016/jceb.2003.11.009)
57. Shimmen T. 2007 The sliding theory of cytoplasmic streaming: fifty years of progress. *J. Plant Res.* **120**, 31–43. (doi:10.1007/s10265-006-0061-0)
58. Nebenführ A, Gallagher LA, Dunahay TG, Frohlick JA, Mazurkiewicz AM, Meehl JB, Staehelin LA. 1999 Stop-and-go movements of plant Golgi stacks are mediated by the actomyosin system. *Plant Physiol.* **121**, 1127–1142. (doi:10.1104/pp.121.4.1127)
59. Mizukami M, Wada S. 1981 Action spectrum for light-induced chloroplast accumulation in a marine coenocytic green alga, *Bryopsis plumosa*. *Plant Cell Physiol.* **22**, 1245–1255.
60. Mineyuki Y, Furuya M. 1986 Involvement of colchicine-sensitive cytoplasmic element in premitotic nuclear positioning of *Adiantum protonemata*. *Protoplasma* **130**, 83–90. (doi:10.1007/BF01276589)
61. Pickard WF. 1974 Hydrodynamic aspects of protoplasmic streaming in *Chara braunii*. *Protoplasma* **82**, 321–339. (doi:10.1007/BF01275727)
62. Pickard WF. 2003 The role of cytoplasmic streaming in symplastic transport. *Plant Cell Environ.* **26**, 1–15. (doi:10.1046/j.1365-3040.2003.00845.x)
63. Matsumoto K, Takagi S, Nakagaki T. 2008 Locomotive mechanism of *Physarum plasmodia* based on spatiotemporal analysis of protoplasmic streaming. *Biophys. J.* **94**, 2492–2504. (doi:10.1529/biophysj.107.113050)
64. Nakagaki T, Yamada H, Tóth A. 2000 Maze-solving by an amoeboid organism. *Nature* **407**, 470. (doi:10.1038/35035159)
65. Nakagaki T, Kobayashi R, Nishiura Y, Ueda T. 2004 Obtaining multiple separate food sources: behavioural intelligence in the *Physarum plasmodium*. *Proc. R. Soc. Lond. B* **271**, 2305–2310. (doi:10.1098/rspb.2004.2856)
66. Tero A, Takagi S, Saigusa T, Ito K, Bebbler EP, Fricker MD, Yumiki K, Kobayashi R, Nakagaki T. 2010 Rules for biologically inspired adaptive network design. *Science* **327**, 439–442. (doi:10.1126/science.1177894)
67. Mahajan-Miklos S, Cooley L. 1994 Intercellular cytoplasm transport during *Drosophila* oogenesis. *Dev. Biol.* **165**, 336–351. (doi:10.1006/dbio.1994.1257)
68. Palacios IM. 2002 *Kinesin light chain*-independent function of the *Kinesin heavy chain* in cytoplasmic streaming and posterior localisation in the *Drosophila* oocyte. *Development* **129**, 5473–5485. (doi:10.1242/dev.00119)
69. Serbus LR, Cha B-J, Theurkauf WE, Saxton WM. 2005 Dynein and the actin cytoskeleton control kinesin-driven cytoplasmic streaming in *Drosophila* oocytes. *Development* **132**, 3743–3752. (doi:10.1242/dev.01956)
70. Zimyanin VL, Belaya K, Pecreaux J, Gilchrist MJ, Clark A, Davis I, St Johnston D. 2008 *In vivo* imaging of oskar mRNA transport reveals the mechanism of posterior localization. *Cell* **134**, 843–853. (doi:10.1016/j.cell.2008.06.053)
71. Khuc Trong P, Guck J, Goldstein RE. 2012 Coupling of active motion and advection shapes intracellular cargo transport. *Phys. Rev. Lett.* **109**, 028104. (doi:10.1103/PhysRevLett.109.028104)
72. Sieberer B, Emons AMC. 2000 Cytoarchitecture and pattern of cytoplasmic streaming in root hairs of *Medicago truncatula* during development and deformation by nodulation factors. *Protoplasma* **214**, 118–127. (doi:10.1007/BF02524268)
73. Hepler PK, Vidali L, Cheung AY. 2001 Polarized cell growth in higher plants. *Annu. Rev. Cell Dev. Biol.* **17**, 159–187. (doi:10.1146/annurev.cellbio.17.1.159)
74. von Dassow G, Schubiger G. 1994 How an actin network might cause fountain streaming and nuclear migration in the syncytial *Drosophila* embryo. *J. Cell. Biol.* **127**, 1637–1653. (doi:10.1083/jcb.127.6.1637)
75. Miller DD, Lancelle SA, Hepler PK. 1996 Actin microfilaments do not form a dense meshwork in *Lilium longiflorum* pollen tube tips. *Protoplasma* **195**, 123–132. (doi:10.1007/BF01279191)
76. Miller DD, De Ruijter NCA, Emons AMC. 1997 From signal to form: aspects of the cytoskeleton-plasma membrane-cell wall continuum in root hair tips. *J. Exp. Biol.* **48**, 1881–1896. (doi:10.1093/jxb/48.11.1881)
77. Tominaga M, Morita K, Sonobe S, Yokota E, Shimmen T. 1997 Microtubules regulate the organization of actin filaments at the cortical region in root hair cells of *Hydrocharis*. *Protoplasma* **199**, 83–92. (doi:10.1007/BF02539809)
78. Vidali L, Hepler PK. 2001 Actin and pollen tube growth. *Protoplasma* **215**, 64–76. (doi:10.1007/BF01280304)
79. Derksen J, Knuiman B, Hoedemaekers K, Guyon A, Bonhomme S, Pierson ES. 2002 Growth and cellular organization of *Arabidopsis* pollen tubes *in vitro*. *Sex Plant Reprod.* **15**, 133–139. (doi:10.1007/s00497-002-0149-1)
80. Lovy-Wheeler A, Cárdenas L, Kunkel JG, Hepler PK. 2007 Differential organelle movement on the actin cytoskeleton in lily pollen tubes. *Cell Motil. Cytoskeleton* **64**, 217–232. (doi:10.1002/cm.20181)
81. Kranz HD, Mikš D, Sieglar M-L, Capesius I, Sensen CW, Huss VAR. 1995 The origin of land plants: phylogenetic relationships among charophytes, bryophytes, and vascular plants inferred from complete small subunit ribosomal RNA gene sequences. *J. Mol. Evol.* **41**, 74–84. (doi:10.1007/BF00174043)
82. Karol KG, McCourt RM, Cimino MT, Delwiche CF. 2001 The closest living relatives of land plants. *Science* **294**, 2351–2353. (doi:10.1126/science.1065156)
83. Shimmen T, Mimura T, Kikuyama M, Tazawa M. 1994 Characean cells as a tool for studying

- electrophysiological characteristics of plant cells. *Cell Struct. Funct.* **9**, 263–278. (doi:10.1247/csf.19.263)
84. Kamiya N, Tazawa M, Takata T. 1963 The relation of turgor pressure to cell volume in *Nitella* with special reference to mechanical properties of the cell wall. *Protoplasma* **57**, 501–521. (doi:10.1007/BF01252073)
85. Green PB, Stanton FW. 1967 Turgor pressure: direct manometric measurement in single cells of *Nitella*. *Science* **155**, 1675–1676. (doi:10.1126/science.155.3770.1675)
86. Green PB, Erickson RO, Buggy J. 1971 Metabolic and physical control of cell elongation rate: *in vivo* studies in *Nitella*. *Plant Physiol.* **47**, 423–430. (doi:10.1104/pp.47.3.423)
87. Zhu GL, Boyer JS. 1992 Enlargement in *Chara* studied with a turgor clamp: growth rate is not determined by turgor. *Plant Physiol.* **100**, 2071–2080. (doi:10.1104/pp.100.4.2071)
88. Proseus TE, Zhu GL, Boyer JS. 2000 Turgor, temperature and the growth of plant cells: using *Chara corallina* as a model system. *J. Exp. Bot.* **51**, 1481–1494. (doi:10.1093/jexbot/51.350.1481)
89. Proseus TE, Boyer JS. 2006 Calcium pectate chemistry controls growth rate of *Chara corallina*. *J. Exp. Bot.* **57**, 3989–4002. (doi:10.1093/jxb/erl166)
90. Proseus TE, Boyer JS. 2007 Tension required for pectate chemistry to control growth in *Chara corallina*. *J. Exp. Bot.* **58**, 4283–4292. (doi:10.1093/jxb/erm318)
91. Wasteneys GO, Williamson RE. 1992 Microtubule organization differs between acid and alkaline bands in internodal cells of *Chara* but bands can develop in the absence of microtubules. *Planta* **188**, 99–105. (doi:10.1007/BF00198945)
92. Wasteneys GO, Williamson RE. 1992 Cortical microtubule organization and internodal cell maturation in *Chara corallina*. *Bot. Acta* **106**, 136–142. (doi:10.1111/j.1438-8677.1993.tb00349.x)
93. Wasteneys GO, Gunning BES, Hepler PK. 1993 Microinjection of fluorescent brain tubulin reveals dynamic properties of cortical microtubules in living plant cells. *Cell Motil. Cytoskeleton* **24**, 205–213. (doi:10.1002/cm.970240308)
94. Wasteneys GO, Collings DA, Gunning BES, Hepler PK, Menzel D. 1996 Actin in living and fixed characean internodal cells: identification of a cortical array of fine actin strands and chloroplast actin rings. *Protoplasma* **190**, 25–38. (doi:10.1007/BF01281192)
95. Kropf DL, Williamson RE, Wasteneys GO. 1997 Microtubule orientation and dynamics in elongating characean internodal cells following cytosolic acidification, induction of pH bands, or premature growth arrest. *Protoplasma* **197**, 188–198. (doi:10.1007/BF01288028)
96. Braun M, Wasteneys GO. 1998 Distribution and dynamics of the cytoskeleton in graviresponding protonemata and rhizoids of characean algae: exclusion of microtubules and a convergence of actin filaments in the apex suggest an actin-mediated gravitropism. *Planta* **205**, 39–50. (doi:10.1007/s004250050294)
97. Foissner I, Wasteneys GO. 1999 Microtubules at wound sites of *Nitella* internodal cells passively co-align with actin bundles when exposed to hydrodynamic forces generated by cytoplasmic streaming. *Planta* **208**, 480–490. (doi:10.1007/s004250050585)
98. Lucas WJ. 1975 Photosynthetic fixation of <sup>14</sup>Carbon by internodal cells of *Chara corallina*. *J. Exp. Bot.* **26**, 331–346. (doi:10.1093/jxb/26.3.331)
99. Ding D-Q, Tazawa M. 1989 Influence of cytoplasmic streaming and turgor pressure gradient on the transnodal transport of rubidium and electrical conductance in *Chara corallina*. *Plant Cell Physiol.* **30**, 739–7489.
100. Kikuyama M, Hara Y, Shimada K, Yamamoto K, Hiramoto Y. 1992 Intercellular transport of macromolecules in *Nitella*. *Plant Cell Physiol.* **33**, 413–417.
101. Franceschi VR, Ding B, Lucas WJ. 1992 Mechanism of plasmodesmata formation in characean algae in relation to evolution of intercellular communication in higher plants. *Planta* **192**, 347–358.
102. Lucas WJ. 1995 Plasmodesmata: intercellular channels for macromolecular transport in plants. *Curr. Opin. Cell Biol.* **7**, 673–680. (doi:10.1016/0955-0674(95)80109-X)
103. Blackman LM, Overall RL. 1998 Immunolocalisation of the cytoskeleton to plasmodesmata of *Chara corallina*. *Plant J.* **14**, 733–741. (doi:10.1046/j.1365-313x.1998.00161.x)
104. van den Berg MS, Coops H, Simons J, de Keizer A. 1998 Competition between *Chara aspera* and *Potamogeton pectinatus* as a function of temperature and light. *Aquat. Bot.* **60**, 241–250. (doi:10.1016/S0304-3770(97)00099-5)
105. Chen Q, Mynett AE, Minns AW. 2002 Application of cellular automata to modelling competitive growths of two underwater species. *Ecol. Model.* **147**, 253–265. (doi:10.1016/S0304-3800(01)00428-8)
106. Kufel L, Kufel I. 2002 *Chara* beds acting as nutrient sinks in shallow lakes: a review. *Aquat. Bot.* **72**, 249–260. (doi:10.1016/S0304-3770(01)00204-2)
107. Siong K, Aasaeda T. 2006 Does calcite encrustation in *Chara* provide a phosphorus nutrient sink? *J. Environ. Quality* **35**, 490–494. (doi:10.2134/jeq2005.0276)
108. Rodrigo M, Rojo C, Alvarezcobelas M, Cirujano S. 2007 *Chara hispida* beds as a sink of nitrogen: evidence from growth, nitrogen uptake and decomposition. *Aquat. Bot.* **87**, 7–14. (doi:10.1016/j.aquabot.2007.01.007)
109. Taiz L. 1992 The plant vacuole. *J. Exp. Biol.* **172**, 113–122.
110. Tazawa M, Kishimoto U. 1964 Studies on *Nitella* having artificial cell sap II. Rate of cyclosis and electric potential. *Plant Cell Physiol.* **5**, 45–59.
111. Foissner I. 2004 Microfilaments and microtubules control the shape, motility, and subcellular distribution of cortical mitochondria in characean internodal cells. *Protoplasma* **224**, 145–157. (doi:10.1007/s00709-004-0075-1)
112. Kachar B, Reese TS. 1988 The mechanism of cytoplasmic streaming in characean algal cells: sliding of endoplasmic reticulum along actin filaments. *J. Cell. Biol.* **106**, 1545–1552. (doi:10.1083/jcb.106.5.1545)
113. Lucas WJ, Ding B, van der Schoot C. 1993 Plasmodesmata and the supracellular nature of plants. *New Phytol.* **125**, 435–476. (doi:10.1111/j.1469-8137.1993.tb03897.x)
114. Goldstein RE, Tuval I, van de Meent J-W. 2008 Microfluidics of cytoplasmic streaming and its implications for intracellular transport. *Proc. Natl Acad. Sci. USA* **105**, 3663–3667. (doi:10.1073/pnas.0707223105)
115. van De Meent JW, Tuval I, Goldstein RE. 2008 Nature's microfluidic transporter: rotational cytoplasmic streaming at high Péclet numbers. *Phys. Rev. Lett.* **101**, 178102. (doi:10.1103/PhysRevLett.101.178102)
116. van De Meent J-W, Sederman AJ, Gladden LF, Goldstein RE. 2010 Measurement of cytoplasmic streaming in single plant cells by magnetic resonance velocimetry. *J. Fluid Mech.* **642**, 5–14. (doi:10.1017/S0022112009992187)
117. Pickard WF. 1972 Further observations on cytoplasmic streaming in *Chara braunii*. *Can. J. Bot.* **50**, 703–711. (doi:10.1139/b72-087)
118. Green PB. 1954 The spiral growth pattern of the cell wall in *Nitella axillaris*. *Am. J. Bot.* **41**, 403–409. (doi:10.2307/2438730)
119. Kamiya N, Kuroda K. 1956 Velocity distribution of the protoplasmic streaming in *Nitella* cells. *Bot. Mag. Tokyo* **69**, 544–554. (doi:10.15281/jplantres1887.69.544)
120. Mustacich RV, Ware BR. 1977 Velocity distributions of the streaming protoplasm in *Nitella flexilis*. *Biophys. J.* **17**, 229–241. (doi:10.1016/S0006-3495(77)85652-X)
121. Woodhouse FG, Goldstein RE. 2012 Shear-driven circulation patterns in lipid membrane vesicles. *J. Fluid Mech.* **705**, 65–175. (doi:10.1017/jfm.2012.118)
122. Honerkamp-Smith AR, Woodhouse FG, Kantsler V, Goldstein RE. 2013 Membrane viscosity determined from shear-driven flow in giant vesicles. *Phys. Rev. Lett.* **111**, 038103. (doi:10.1103/PhysRevLett.111.038103)
123. Raven JA. 1987 The role of vacuoles. *New Phytol.* **106**, 357–422. (doi:10.1111/j.1469-8137.1987.tb00149.x)
124. Coops H. 2002 Ecology of charophytes: an introduction. *Aquat. Bot.* **72**, 205–208. (doi:10.1016/S0304-3770(01)00200-5)
125. Green PB. 1958 Structural characteristics of developing *Nitella* internodal cell walls. *J. Biophys. Biochem. Cytol.* **4**, 505–515. (doi:10.1083/jcb.4.5.505)
126. Shepherd VA, Goodwin PB. 1992 Seasonal patterns of cell-to-cell communication in *Chara corallina* Klein ex Willd. II. Cell-to-cell communication during the development of antheridia. *Plant Cell Env.* **15**, 151–162. (doi:10.1111/j.1365-3040.1992.tb01469.x)
127. Bostrom TE, Walker NA. 1975 Intercellular transport in plants. I. The rate of transport of chloride and the

- electric resistance. *J. Exp. Bot.* **26**, 767–782. (doi:10.1093/jxb/26.6.767)
128. Williams EJ, Fensom DS. 1975 Axial and transnodal movement of  $^{14}\text{C}$ ,  $^{22}\text{Na}$ , and  $^{36}\text{Cl}$  in *Nitella translucens*. *J. Exp. Bot.* **26**, 783–807. (doi:10.1093/jxb/26.6.783)
129. Zawadzki T, Fensom DS. 1986 Transnodal transport of  $^{14}\text{C}$  in *Nitella flexilis* I. Tandem cells without applied pressure gradients. *J. Exp. Bot.* **37**, 1341–1352. (doi:10.1093/jxb/37.9.1341)
130. Zawadzki T, Fensom DS. 1986 Transnodal transport of  $^{14}\text{C}$  in *Nitella flexilis* II. Tandem cells with applied pressure gradients. *J. Exp. Bot.* **37**, 1341–1352. (doi:10.1093/jxb/37.9.1353)
131. Trebacz K, Fensom DS, Harris A, Zawadzki T. 1988 Transnodal transport of  $^{14}\text{C}$  in *Nitella flexilis* III. Further studies on dissolved inorganic carbon movements in tandem cells. *J. Exp. Bot.* **39**, 1561–1573. (doi:10.1093/jxb/39.11.1561)
132. Littlefield L, Forsberg C. 1965 Absorption and translocation of phosphorus-32 by *Chara globularis* Thuill. *Physiol. Plantarum* **18**, 291–293. (doi:10.1111/j.1399-3054.1965.tb06891.x)
133. Box RJ. 1986 Quantitative short-term uptake of inorganic phosphate by the *Chara hispida* rhizoid. *Plant Cell Environ.* **9**, 501–506. (doi:10.1111/j.1365-3040.1986.tb01767.x)
134. Box RJ. 1987 The uptake of nitrate and ammonium nitrogen in *Chara hispida* L.: the contribution of the rhizoid. *Plant Cell Environ.* **10**, 169–176. (doi:10.1111/j.1365-3040.1987.tb02094.x)
135. Vermeer CP, Escher M, Portielje M, de Klein JJM. 2003 Nitrogen uptake and translocation by *Chara*. *Aquat. Bot.* **76**, 245–258. (doi:10.1016/S0304-3770(03)00056-1)
136. Forsberg C. 1965 Nutritional studies of *Chara* in axenic cultures. *Physiol. Plantarum* **18**, 275–291. (doi:10.1111/j.1399-3054.1965.tb06890.x)
137. Ding DQ, Nagata T, Amino S, Tazawa M. 1991 Intercellular transport and subcellular distribution of photoassimilates in *Chara corallina*. *J. Exp. Bot.* **42**, 1393–1398. (doi:10.1093/jxb/42.11.1393)
138. Ding DQ, Mimura T, Amino S, Tazawa M. 1991 Intercellular transport and photosynthetic differentiation in *Chara corallina*. *J. Exp. Bot.* **42**, 33–38. (doi:10.1093/jxb/42.1.33)
139. Shepherd VA, Goodwin PB. 1992 Seasonal patterns of cell-to-cell communication in *Chara corallina* Klein ex Willd. I. Cell-to-cell communication in vegetative lateral branches during winter and spring. *Plant Cell Environ.* **15**, 137–150. (doi:10.1111/j.1365-3040.1992.tb01468.x)
140. Bostrom TE, Walker NA. 1976 Intercellular transport in plants II. Cyclosis and the rate of intercellular transport of chloride in *Chara*. *J. Exp. Bot.* **27**, 347–357. (doi:10.1093/jxb/27.2.347)
141. Dale N, Lunn G, Fensom DS, Williams EJ. 1983 Rates of axial transport of  $^{11}\text{C}$  and  $^{14}\text{C}$  in Characean cells: faster than visible streaming? *J. Exp. Bot.* **34**, 130–143. (doi:10.1093/jxb/34.2.130)
142. Box R, Andrews M, Raven JA. 1984 Intercellular transport and cytoplasmic streaming in *Chara hispida*. *J. Exp. Bot.* **35**, 1016–1021. (doi:10.1093/jxb/35.7.1016)
143. Tazawa M, Shimmen T, Mimura T. 1987 Membrane control in the Characeae. *Annu. Rev. Plant Physiol.* **38**, 95–117. (doi:10.1146/annurev.pp.38.060187.000523)
144. Plieth C, Tabrizi H, Hansen UP. 1994 Relationship between banding and photosynthetic activity in *Chara corallina* as studied by the spatially different induction curves of chlorophyll fluorescence observed by an image analysis system. *Physiol. Plantarum* **91**, 205–211. (doi:10.1111/j.1399-3054.1994.tb00420.x)
145. McConnaughey TA, Falk RH. 1991 Calcium-proton exchange during algal calcification. *Biol. Bull.* **180**, 185–195. (doi:10.2307/1542440)
146. McConnaughey T. 1991 Calcification in *Chara corallina*:  $\text{CO}_2$  hydroxylation generates protons for bicarbonate assimilation. *Limnol. Oceanogr.* **36**, 619–628. (doi:10.4319/lo.1991.36.4.0619)
147. McConnaughey T. 1998 Acid secretion, calcification, and photosynthetic carbon concentrating mechanisms. *Can. J. Bot.* **76**, 1119–1126. (doi:10.1139/b98-066)
148. Mimura T, Müller R, Kaiser WM, Shimmen T, Dietz K-J. 1993 ATP-dependent carbon transport in perfused *Chara* cells. *Plant Cell Environ.* **16**, 653–661. (doi:10.1111/j.1365-3040.1993.tb00483.x)
149. Bulychev AA, Vredenberg W. 2003 Spatiotemporal patterns of photosystem II activity and plasma-membrane proton flows in *Chara corallina* cells exposed to overall and local illumination. *Planta* **218**, 143–151. (doi:10.1007/s00425-003-1084-6)
150. Bulychev AA, van Den Wijngaard PWJ, de Boer AH. 2005 Spatial coordination of chloroplast and plasma membrane activities in chara cells and its disruption through inactivation of 14-3-3 proteins. *Biochemistry (Moscow)* **70**, 55–61. (doi:10.1007/s10541-005-0051-1)
151. Babourina O, Voltchanskii K, Newman I. 2004 Ion flux interaction with cytoplasmic streaming in branchlets of *Chara australis*. *J. Exp. Bot.* **55**, 2505–2512. (doi:10.1093/jxb/erh256)
152. Lucas WJ, Dainty J. 1977 Spatial distribution of functional  $\text{OH}^-$  carriers along a characean internodal cell: determined by the effect of cytochalasin B on  $^{14}\text{HCO}_3^-$  assimilation. *J. Membr. Biol.* **32**, 75–92. (doi:10.1007/BF01905210)
153. Eremin A, Bulychev A, Krupenina NA, Mair T, Hauser MJB, Stannarius R, Müller SC, Rubin AB. 2007 Excitation-induced dynamics of external pH pattern in *Chara corallina* cells and its dependence on external calcium concentration. *Photochem. Photobiol. Sci.* **6**, 103–109. (doi:10.1039/B607602E)
154. Toko H, Chosa H, Yamafuji K. 1985 Dissipative structure in the Characeae: spatial pattern of proton flux as a dissipative structure in characean cells. *J. Theor. Biol.* **114**, 125–175. (doi:10.1016/S0022-5193(85)80260-5)
155. Dinh AT, Pangarkar C, Theofanous T, Mitragotri S. 2006 Theory of spatial patterns of intracellular organelles. *Biophys. J.* **90**, L67–L69. (doi:10.1529/biophysj.106.082875)
156. Snider J, Lin F, Rodionov B, Yu CC, Gross SP. 2004 Intracellular actin-based transport: how far you go depends on how often you switch. *Proc. Natl Acad. Sci. USA* **101**, 1355–1357. (doi:10.1073/pnas.0403092101)
157. Maly IV. 2002 A stochastic model for patterning of the cytoplasm by the saltatory movement. *J. Theor. Biol.* **216**, 59–71. (doi:10.1006/jtbi.2002.2531)
158. Smith DA, Simmons RM. 2001 Models of motor-assisted transport of intracellular particles. *Biophys. J.* **80**, 45–68. (doi:10.1016/S0006-3495(01)75994-2)
159. Houtman D, Pagonabarraga I, Lowe CP, Esseling-Ozboda A, Emons AMC, Eiser E. 2007 Hydrodynamic flow caused by active transport along cytoskeletal elements. *Europhys. Lett.* **78**, 18001. (doi:10.1209/0295-5075/78/18001)
160. Tazawa M, Kishimoto U. 1968 Cessation of cytoplasmic streaming of *Chara* internodes during action potential. *Plant Cell Physiol.* **9**, 361–368.
161. Tazawa M. 1964 Studies on *Nitella* having artificial cell sap. I. Replacement of the cell sap with artificial solutions. *Plant Cell Physiol.* **5**, 33–43.
162. Kamiya N, Kuroda K. 1958 Measurement of the motive force of the protoplasmic rotation in *Nitella*. *Protoplasma* **50**, 144–148. (doi:10.1007/BF01666244)
163. Tazawa M. 1968 Motive force of the cytoplasmic streaming in *Nitella*. *Protoplasma* **65**, 207–222. (doi:10.1007/BF01666379)
164. Mustacich RV, Ware BR. 1976 A study of protoplasmic streaming in *Nitella* by laser Doppler spectroscopy. *Biophys. J.* **16**, 373–388. (doi:10.1016/S0006-3495(76)85695-0)
165. Donaldson IG. 1972 The estimation of the motive force for protoplasmic streaming in *Nitella*. *Protoplasma* **74**, 329–344. (doi:10.1007/BF01282536)
166. Hayashi Y. 1980 Fluid-dynamical study of protoplasmic streaming in a plant cell. *J. Theor. Biol.* **85**, 451–467. (doi:10.1016/0022-5193(80)90319-7)
167. Kamiya N, Kuroda K. 1963 Rotational protoplasmic streaming in *Nitella* and some physical properties of the endoplasm. In *Proc. Fourth Int. Congress on Rheology, Part 4, Symposium on Biorheology*, pp. 157–171, New York, NY: John Wiley & Sons.
168. Nothnagel EA, Webb WW. 1982 Hydrodynamic models of viscous coupling between motile myosin and endoplasm in characean algae. *J. Cell Biol.* **94**, 444–454. (doi:10.1083/jcb.94.2.444)
169. Wolff K, Marenduzzo D, Cates ME. 2012 Cytoplasmic streaming in plant cells: the role of wall slip. *J. R. Soc. Interface* **9**, 1398–1408. (doi:10.1098/rsif.2011.0868)
170. de Vries H. 1885 Über die Bedeutung der Cirkulation und der Rotation des Protoplasma für den Stofftransport in der Pflanze. *Bot. Ztg.* **43**, 1–6, 17–26.
171. van de Meent J-W. 2010 Making it big; how characean algae use cytoplasmic streaming to enhance transport in giant cells. Doctoral thesis, Universiteit Leiden, The Netherlands.

172. Yotsuyanagi Y. 1953 Recherches sur les phénomènes moteurs dans les fragments de protoplasme isolés. I. Mouvement rotatoire et le processus de son apparition. *Cytologia* **18**, 146–156. (doi:10.1508/cytologia.18.146)
173. Foissner I, Wasteneys GO. 2000 Microtubule disassembly enhances reversible cytochalasin-dependent disruption of actin bundles in characean internodes. *Protoplasma* **214**, 33–44. (doi:10.1007/BF02524260)
174. Woodhouse FG, Goldstein RE. 2013 Cytoplasmic streaming in plant cells emerges naturally by microfilament selforganization. *Proc. Natl Acad. Sci. USA* **110**, 14 132–14 137. (doi:10.1073/pnas.1302736110)
175. Woodhouse FG, Goldstein RE. 2012 Spontaneous circulation of confined active suspensions. *Phys. Rev. Lett.* **109**, 168105. (doi:10.1103/PhysRevLett.109.168105)
176. Wioland H, Woodhouse FG, Dunkel J, Kessler JO, Goldstein RE. 2013 Confinement stabilizes a bacterial suspension into a spiral vortex. *Phys. Rev. Lett.* **110**, 268102. (doi:10.1103/PhysRevLett.110.268102)
177. Lushi E, Wioland H, Goldstein RE. 2014 Fluid flows created by swimming bacteria drive self-organization in confined suspensions. *Proc. Natl Acad. Sci. USA* **111**, 9733–9738. (doi:10.1073/pnas.1405698111)